



# Corrections applied to direct shear results and development of modified Barton's shear strength criterion for rock joints

Rakesh Kumar<sup>1</sup> · Abhiram Kumar Verma<sup>1</sup>

Received: 15 November 2018 / Accepted: 15 September 2020 / Published online: 24 September 2020  
 © Saudi Society for Geosciences 2020

## Abstract

In present study, 144 direct shear tests are performed on mated rock joint replicas under constant normal load condition (CNL). For these tests, three natural roughness of joint surface are transferred to the RTV silicon rubber molds. On these molds, mixture of cement, sand, and water in the ratio of 1:1.5:0.45 by weight is poured and joint replicas are made. In this study, the experimental shear strength is corrected with gross contact area ( $A_c$ ) and incremental dilation angle ( $i$ ). Further, the peak dilation angle is determined by Barton's and incremental dilation ( $dv/dh$ ) approaches and compared. The results showed that Barton's approach underestimates the peak dilation angle. The roughness quantification of joint surface is done using 3D noncontact type profiler, and morphological parameters of joint surface are determined in each shearing direction as described by Grasselli and Egger (Int J Rock Mech Min Sci 40:25–40, 2003). A new predictive model for joint roughness coefficient (JRC) is developed and Barton's model is modified. It is observed that modified Barton's model provides good approximation of shear strength in desired shear direction. Moreover, modified Barton peak shear strength ( $\tau_{Pre}$ ) is compared with Barton and Grasselli's experimental peak shear strength, and it is observed that  $\tau_{Pre}$  matches closely with Barton's peak shear strength.

**Keywords** Incremental dilation angle · Direct shear test · Maximum asperity angle · Joint roughness coefficient

## List of symbol

$\sigma_n$	Normal stress
$\phi_b$	Basic friction angle
$\tau_i$	Dilation corrected shear stress
$\tau_{ip}$	Dilation corrected peak shear stress
$\tau$ or $\tau_{exp}$	Experimental or uncorrected shear stress
$\tau_A$	Gross contact area corrected shear stress
$\tau_{Pre}$	Modified Barton peak shear strength
$\tau_B$	Barton's peak shear strength
$\tau_p$	Uncorrected peak shear stress
$\tau_{GE}$	Grasselli's experimental shear strength

$A$	Amplitude of profile
$CNL$	Constant normal load
$D$	Fractal dimension
$JRC$	Joint roughness coefficient
$JCS$	Joint wall compressive strength
$L$	Length of sample
$RTV$	Room temperature vulcanizing
$Z_2$	Root mean square of first derivative of profile
$dy/dx$	Slope of profile
$A_c$	Gross contact area
$A_{\theta^*}$	Normalized potential contact area
$A_0$	Maximum potential contact area
$\theta_{max}$	Maximum asperity angle
$\theta^*$	Threshold dip angle
$C$	Dimensionless fitting parameters
$i$	Incremental dilation angle
$r$	Radius of sample
$dv/dh$	Rate of dilation
$d_n$	Dilation angle
$d_{na}$	Actual peak dilation angle
$SSE$	Sum of square error
$MSE$	Mean square error
$N$	No. of data

Responsible Editor: Zeynal Abiddin Erguler

✉ Abhiram Kumar Verma  
 akverma@mining.iitkgp.ac.in; abhiram.verma@gmail.com

Rakesh Kumar  
 rkumar@mining.iitkgp.ac.in

<sup>1</sup> Department of Mining Engineering, Indian Institute of Technology Kharagpur, Kharagpur, West Bengal, India

## Introduction

Rock mass contains many types of discontinuities like fault, fold, and joints. ISRM (1978) defines these discontinuities as having zero tensile strength. Among them, joint can be defined as a plane of weakness along which there is no visible displacement. It can be opened or filled with gouge material such as silt and clay. The presence of rock joints largely governs the mechanical properties of rock mass. In geotechnical engineering, the accurate assessment of joint shear strength is very essential for stability of rock mass. The shear strength is mostly controlled by the roughness of joint surface which is composed of first-order (waviness) and second-order (unevenness) asperities.

Due to very complex nature of roughness, the accurate prediction of joint shear strength is not an easy task. In literature, many constitutive models (Patton 1966; Ladanyi and Archambault 1970; Barton 1973; Plesha et al. 1989; Maksimović 1992, 1996; Jing et al. 1992; Huang et al. 1993; Wibowo et al. 1994; Kulatilake et al. 1995; Zhao 1997a, b; Amadei et al. 1998; Yang and Chiang 2000; Indraratna and Haque 2000; Homand et al. 2001; Wang et al. 2003; Grasselli and Egger 2003; Tatone 2009; Asadollahi and Tonon 2010; Ghazvinian et al. 2012; Xia et al. 2014) are developed to predict shear strength of rock joints under CNL condition. Among all constitutive models, Barton model (Eq. 1) is still widely used in practice due to its simplicity.

$$\tau_B = \sigma_n \tan \left[ \phi_b + JRC \log_{10} \left( \frac{JCS}{\sigma_n} \right) \right] \quad (1)$$

where  $\phi_b$  is the basic friction angle,  $JRC$  is the joint roughness coefficient, and  $JCS$  is the joint wall strength which is equal to compressive strength of rock for fresh rock joints.  $JRC$  can be estimated either by back calculation of direct shear tests results or by visual comparison with ten standard profiles ranging from 0 to 20 (Barton and Choubey 1977).

In the field of rock engineering, the accurate determination of  $JRC$  remains an active area of research, and to quantify  $JRC$ , several methods like statistical (Tse and Cruden 1979; Yu and Vayssade 1991; Yang et al. 2001; Tatone and Grasselli 2010), fractal (Brown and Scholz 1985; Reeves 1985; Maerz et al. 1990; Milinverno 1990; Power and Tullis 1991; Sakellariou et al. 1991; Huang et al. 1992; Odling 1994; Kulatilake and Um 1999; Xie et al. 1999; Yang and Di 2001), and tilt tests (Barton et al. 1985) are used in literature.

Tse and Cruden (1979) proposed empirical statistical relationship between the  $JRC$  and  $Z_2$  (root mean square of first derivative of profile). In their study, ten standard profiles given by Barton and Choubey (1977) are enlarged by 2.5 times both in x and y coordinates. Then, new profile (25 cm long) digitized along its length and 200 discrete data points taken at equal interval of 1.27 mm. However, the enlargement of standard profiles seems incorrect because it changes the roughness

of profile significantly, but Tse and Cruden's relationship (Eq. 2) is still used as an alternate method to estimate  $JRC$  numerically.

$$JRC = 32.2 + 32.47 \log_{10} Z_2 \quad (2)$$

where  $Z_2$  is given as:

$$Z_2 = \sqrt{\frac{1}{L} \int_{x=0}^{x=L} \left( \frac{dy}{dx} \right)^2 dx} = \sqrt{\frac{1}{L} \sum_{i=1}^{i=N-1} \frac{(y_{i+1} - y_i)^2}{(x_{i+1} - x_i)}} \quad (3)$$

In Eq. 3,  $L$  is length of profile and  $dy/dx$  is the slope of profile at fixed interval. The value of  $Z_2$  is not unique and it is sensitive to choice of sampling interval. The relationships between  $JRC$  and  $Z_2$  at different sampling interval are studied by many researchers as given in Table 1.

In literature, fractal methods (Brown and Scholz 1985; Reeves 1985; Maerz et al. 1990; Milinverno 1990; Power and Tullis 1991; Sakellariou et al. 1991; Huang et al. 1992; Odling 1994; Kulatilake and Um 1999; Xie et al. 1999; Yang and Di 2001) are used for estimation of  $JRC$ . Odling (1994) determined the amplitude ( $A$ ) and fractal dimension ( $D$ ) of ten standard profiles and observed that with increase in  $JRC$ , amplitude ( $A$ ) of profiles increases while fractal dimension ( $D$ ) decreases. He showed that rough joints and smoother joints have  $D$  values close to 1 (self-similar fractal) and 1.5 (self-affine fractal), respectively. Khosravi et al. (2013) measures " $D$ " for saw toothed joint samples with line segment method and establish power relationship between back calculated  $JRC$  and " $D$ ." Li and Huang (2015) had done review of compass-walking, box-counting, and average height-base length (h-b) methods for determining " $D$ " of ten standard profiles and discussed applicability of existing relationships of  $JRC$  and  $D$  in literature. They indicate that the fractal dimension estimated from compass-walking and h-b method more closely relate to  $JRC$  than box-counting methods.

Grasselli and Egger (2003) and Tatone (2009) developed new surface characterization parameters and shown that normalized potential contact area ( $A_{\theta^*}$ ) in specific shear direction is function of threshold dip angle ( $\theta^*$ ) as shown in Eq. 4.

$$A_{\theta^*} = A_0 \left( \frac{\theta_{max} - \theta^*}{\theta_{max}} \right)^C \quad (4)$$

where  $A_0$  is the maximum potential contact area for specified shear direction which is found by putting threshold dip angle ( $\theta^*$ ) equal to zero,  $\theta_{max}$  is the maximum asperity angle in shear direction, and  $C$  is the dimensionless fitting parameters that characterize the distribution of apparent inclination angles over the joint surface in desired shear direction. Moreover, they postulated that parameters ( $A_0$ ,  $\theta_{max}$ , and  $C$ ) are directional dependent, and the ratio of  $\theta_{max}/(C+1)$  is capable to characterize the anisotropy in roughness of joint surface.

**Table 1** Existing relationship of  $Z_2$  with  $JRC$  in literature

Authors	Proposed relationships	Sampling interval (mm)
Yu and Vayssade (1991)	$JRC = 60.32 Z_2 - 4.51$	0.25
Yu and Vayssade (1991)	$JRC = 61.79 Z_2 - 3.47$	0.50
Yu and Vayssade (1991)	$JRC = 64.22 Z_2 - 2.31$	1.00
Yang et al. (2001)	$JRC = 32.69 + 32.98 \log_{10} Z_2$	0.50
Tatone and Grasselli (2010)	$JRC = 51.85(Z_2)^{0.60} - 10.37$	0.50
Tatone and Grasselli (2010)	$JRC = 55.03(Z_2)^{0.74} - 6.10$	1.00

In literature, many empirical equations are available to find  $JRC$  based on statistical parameter and the fractal dimension. In these empirical equations, one of the major drawback is that  $JRC$  values are taken from Barton’s standard ten 2D profiles of 10 cm which subjective in nature. Moreover, it is almost impossible to compare a 3D joint surface with these standard profiles. Therefore, in this study, to eliminate subjectivity in estimation of  $JRC$ , a predictive model is proposed based on known morphological parameter of joint surface in desired shear direction.

The experimental shear stress or uncorrected shear stress ( $\tau$ ) is simply the shear force divided by nominal (fixed) area. Many researchers (Hencher and Richards 1989; Jing et al. 1992; Muralha et al. 2014) suggested that sample half that remains fixed during shearing should have greater diameter than the moving half sample so that nominal area remains constant throughout the test. If this procedure is not followed then nominal area or gross contact area reduction techniques should be carried out for estimation of correct shear stress. Moreover, due to complex nature of roughness, angle of shearing plane continuously changes during the direct shear tests. This leads to continuous change in dilation angle. Therefore, in this manuscript, experimental peak shear strength is corrected with gross contact area ( $A_C$ ) and incremental dilation angle ( $i$ ) and a correct method to find peak dilation angle is also discussed.

### Sample preparation

The natural rock joint samples are collected from different location and three different profiles of 90-mm diameter are

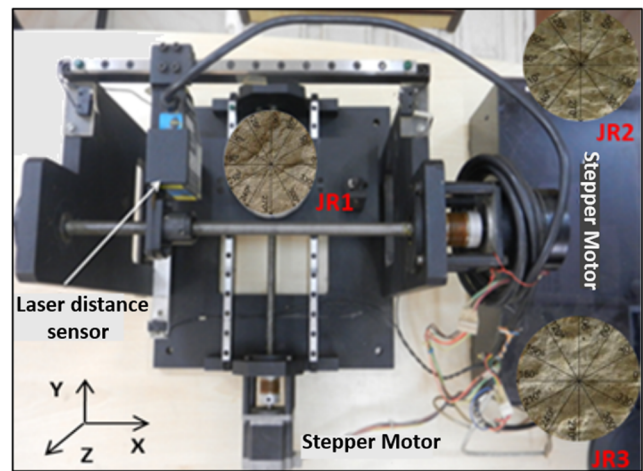


**Fig. 1** 3D noncontact type joint surface profiler used for roughness quantification of replicas

selected visually on them. The joint roughness is transferred to silicon rubber mold with the help of room temperature vulcanizing (RTV) silicon rubber and catalyst. Further, ratio of cement, sand, and water in the ratio of 1:1.5:0.45 by weight is poured on silicon rubber mold, and finally, joint replicas (JR1, JR2, and JR3) are prepared. The detailed description of sample preparation is given by Kumar and Verma (2016).

The mechanical properties like uniaxial compressive strength, Brazilian tensile strength, and Poisson’s ratio of joint replicas are determined and reported in Table 2. The basic friction angle ( $\phi_b$ ) of replicas are determined on saw cut surface and found to be 35.83°.

### Roughness quantification

A 3D noncontact type rock surface profiler is used for roughness quantification of joint replicas (Fig. 1). It is a laser scanner and has least count of 0.5 mm in X and Y directions and 0.1 mm in Z direction. Each joint replica is scanned at 30° interval in only six directions (0°, 30°, 60°, 90°, 120°, and 150°) because in backward and forward directions, roughness measurement will remain same. In each shearing direction, for 90 mm replica, a total of 180 parallel lines at 0.5 mm spacing were obtained with X, Y, and Z data. These data are processed

**Table 2** Mechanical properties of model material (Kumar and Verma 2016)

Mechanical properties	No of samples	Average value	SD
Uniaxial compressive strength ( $\sigma_c$ )	7	40.83 MPa	1.95
Brazilian tensile strength ( $\sigma_t$ )	7	4.36 MPa	0.37
Poisson’s ratio ( $\nu$ )	3	0.17	0.03
Density ( $\rho$ )	10	21.45 kN/m <sup>3</sup>	0.46
Young modulus ( $E$ )	7	10.09 GPa	0.52
Basic friction angle of rock, ( $\phi_b$ )	1	35.83 Deg	–

in MATLAB software to find joint roughness parameters ( $A_0$ ,  $\theta_{max}$ , and  $C$ ) as suggested by Grasselli and Egger (2003).

To visualize the distribution of  $A_{\theta^*}$  with  $\theta^*$  of asperities ( $0^\circ, 15^\circ, 25^\circ, 35^\circ \dots$ ) over joint surface in shear direction, plots between them are shown in Fig. 2a. These graphs depict maximum potential contact area for particular threshold dip angle before shearing. Further, to determine the value of  $C$ , the graph between  $A_{\theta^*}$  and  $(\theta_{max} - \theta^*)/\theta_{max}$  is plotted and found that these are related in power function (Fig. 2b). Further, nonlinear regression analysis was performed to find the correct value of parameter  $C$  as described (Tatone 2009). The values of  $A_0$  and  $C$  for three joint replicas are reported in Table 3 and observed that these values are comparable with existing values in literature (Grasselli et al. 2002; Xia et al. 2014). It is observed that values of  $A_0$ ,  $C$ , and  $\theta_{max}$  change as shearing direction changes which show the capability to characterize the anisotropy of joint surface.

### Direct shear tests

In this study, a total of 144 direct shear tests are performed using 4 normal stresses (0.25, 0.5, 1.0 and 1.5 MPa) under *CNL* condition. For particular profile and at each normal stress, twelve direct shear tests are performed at  $30^\circ$  apart in anticlockwise direction from direction  $0^\circ$  as shown in Fig. 1. This  $0^\circ$  is marked and kept constant for particular profile. The electro-mechanical direct shear apparatus is used for conducting all shear tests. The joint replicas of 90 mm diameter are put with necessary arrangements in square shear box of 10 cm. These tests are performed up to 10 mm of shear displacement at shearing rate of 0.2 mm/min (Muralha et al. 2014). The shear load, normal load, shear displacement, and

vertical displacement are recorded by a personal computer equipped with a data acquisition system.

## Results and discussion

### Correcting shear stress with gross contact area ( $A_c$ )

It is observed that for any direct shear test, huge data points (around 2000 to 2500) are generated because data are recorded at 1 second interval. Among these data, it is also observed that for the same shear displacements, many close values of shear load and vertical displacement exist. These data are defined as “identical data” in this study. To overcome this issue, Origin Lab version 2018 is used in which these identical data are averaged to get one value of shear load and vertical displacement at particular shear displacement. This procedure reduced the data points (around 1000) which is quite easy for further calculation.

Among these data, the shear load and shear displacement are selected at interval of 0.2 mm with MATLAB program. The value of 0.2 mm shear displacement is so selected that there is minimum loss of data points. Then, corrected shear stress with gross contact area ( $\tau_A$ ) is calculated by dividing the shear force with the gross contact area ( $A_c$ ). For shear displacement of “ $\Delta h$ ” in mm, the gross contact area ( $A_c$ ) is calculated with Eq. 5 (Hencher and Richards 1989).

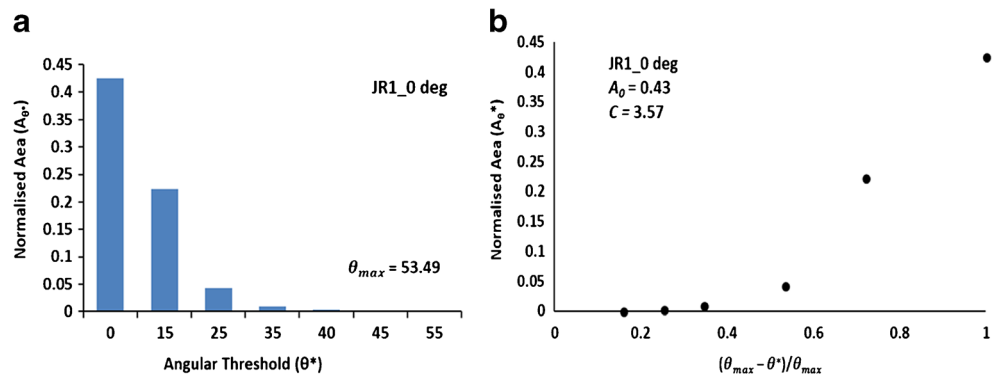
$$A_c = \pi r^2 - \left( \frac{\Delta h r \sqrt{4r^2 - (\Delta h)^2}}{2r} \right) - 2r^2 \sin^{-1} \left( \frac{\Delta h}{2r} \right) \quad (5)$$

where “ $r$ ” is the radius of sample in mm.

**Table 3** Estimated values of  $C$ ,  $\theta_{max}$ , and  $A_0$  for joint replicas

Shearing direction	JR1			JR2			JR3		
	$C$	$\theta_{max}$	$A_0$	$C$	$\theta_{max}$	$A_0$	$C$	$\theta_{max}$	$A_0$
0	3.57	53.49	0.43	3.56	80.31	0.31	3.51	82.06	0.33
30	3.5	62.48	0.42	4.94	84.22	0.28	5.78	84.48	0.32
60	3.14	57.02	0.41	3.22	81.57	0.25	2.78	71.14	0.30
90	5.35	85.22	0.41	2.71	68.58	0.27	2.52	66.51	0.28
120	3.74	53.28	0.41	3.72	81.25	0.29	4.28	73.77	0.28
150	6.95	80.66	0.43	3.99	71.83	0.30	3.05	65.05	0.30
180	4.86	55.43	0.43	3.13	79.92	0.31	4.53	83.49	0.33
210	3.49	66.51	0.42	2.87	82.81	0.28	4.2	86.96	0.32
240	4.14	79.66	0.41	3.62	73.21	0.25	3.84	75.12	0.30
270	4.2	82.89	0.41	1.91	62.72	0.27	2.97	76.83	0.28
300	4.41	55.64	0.41	3.06	86.05	0.29	5.94	78.45	0.28
330	2.95	62.16	0.43	2.61	65.21	0.30	2.29	67.89	0.30

**Fig. 2** (a) Distribution of  $A_{\theta^*}$  with  $\theta^*$  (b) graph between  $A_{\theta^*}$  and  $(\theta_{max} - \theta^*)/\theta_{max}$



**Correcting shear stress with incremental dilation angle (*i*)**

If the shear plane has angle (*i*) from the horizontal, the normal stress ( $\sigma_n$ ) and corrected shear stress with gross contact area ( $\tau_A$ )

can resolved tangentially and vertically to the plane of shearing. Then, dilation corrected shear stress ( $\tau_i$ ) and normal stress ( $\sigma_i$ ) can be evaluated by following equations (Hencher et al. 2011).

$$\tau_i = (\tau_A \cos i - \sigma_n \sin i) \cos i \tag{6}$$

**Table 4** Comparison of peak shear stress ( $\tau_p$ ) and dilation corrected peak shear stress ( $\tau_{ip}$ )

Joint Replica	Shearing direction	$\sigma_{n1} = 0.25$ MPa		$\sigma_{n2} = 0.5$ MPa		$\sigma_{n3} = 1$ MPa		$\sigma_{n4} = 1.5$ MPa	
		$\tau_p$ (MPa)	$\tau_{ip}$ (MPa)	$\tau_p$ (MPa)	$\tau_{ip}$ (MPa)	$\tau_p$ (MPa)	$\tau_{ip}$ (MPa)	$\tau_p$ (MPa)	$\tau_{ip}$ (MPa)
JR1	0	0.48	0.46	0.55	0.56	1.31	1.37	1.47	1.55
	30	0.35	0.35	0.72	0.74	1.08	1.09	1.57	1.57
	60	0.29	0.39	0.51	0.52	0.83	1.15	1.15	1.09
	90	0.41	0.43	0.53	0.65	1.02	1.22	1.50	1.51
	120	0.38	0.38	0.44	0.53	1.05	1.09	1.28	1.58
	150	0.38	0.40	0.64	0.68	1.01	1.05	1.18	1.38
	180	0.57	0.56	0.66	0.67	1.01	1.28	1.76	1.92
	210	0.43	0.45	0.92	0.90	1.39	1.49	2.06	2.23
	240	0.54	0.52	0.95	0.91	1.24	1.25	1.72	1.69
	270	0.39	0.43	0.55	0.48	1.64	1.74	2.08	2.02
	300	0.57	0.56	0.83	0.79	1.22	1.33	1.52	1.64
	330	0.47	0.43	0.92	0.83	1.38	1.28	1.62	1.63
	JR2	0	0.47	0.41	1.14	1.08	1.61	1.81	1.82
30		0.68	0.61	1.11	1.07	1.84	1.67	2.64	2.56
60		0.58	0.66	1.29	1.20	1.99	1.99	3.28	3.36
90		0.50	0.49	0.93	0.88	1.05	0.97	1.87	1.97
120		0.61	0.44	0.83	0.80	0.96	1.01	1.84	1.85
150		0.54	0.54	0.77	0.73	1.45	1.44	2.26	2.25
180		0.50	0.48	0.88	0.80	1.17	1.44	2.10	2.24
210		0.44	0.45	0.67	0.64	1.63	1.64	1.82	2.06
240		0.47	0.45	1.10	1.04	1.15	1.13	2.22	2.37
270		0.40	0.43	0.96	0.92	1.43	1.48	2.39	2.45
300		0.54	0.61	0.68	0.69	1.30	1.35	1.98	2.20
330		0.67	0.65	0.99	0.93	1.89	1.80	2.74	2.66
JR3		0	0.45	0.43	0.74	0.74	1.04	1.08	1.48
	30	0.46	0.44	0.76	0.74	1.01	1.04	1.85	1.83
	60	0.58	0.59	0.96	0.89	1.46	1.01	2.10	1.90
	90	0.43	0.40	1.14	0.97	1.73	1.73	2.32	2.22
	120	0.64	0.65	1.33	1.33	1.87	1.67	2.29	2.22
	150	0.45	0.46	0.68	0.79	1.41	1.49	2.34	2.35
	180	0.50	0.48	0.71	0.73	1.13	1.12	2.09	2.24
	210	0.41	0.43	0.74	0.76	1.11	1.16	1.70	1.81
	240	0.39	0.35	0.87	0.84	1.48	1.53	1.94	1.99
	270	0.58	0.56	0.83	0.76	1.24	1.16	1.57	1.68
	300	0.47	0.44	0.90	0.91	1.25	1.26	1.41	1.45
	330	0.40	0.35	0.79	0.74	1.35	1.32	1.95	2.00

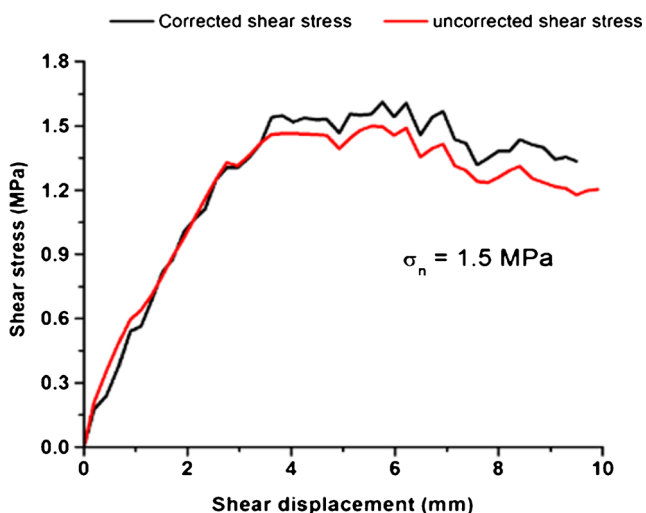


Fig. 3 Comparison of dilation corrected shear stress ( $\tau_i$ ) and uncorrected shear stress ( $\tau_{exp}$ ) in  $0^\circ$  direction of JR1

$$\sigma_i = (\sigma_n \cos i + \tau_A \sin i) \cos i \tag{7}$$

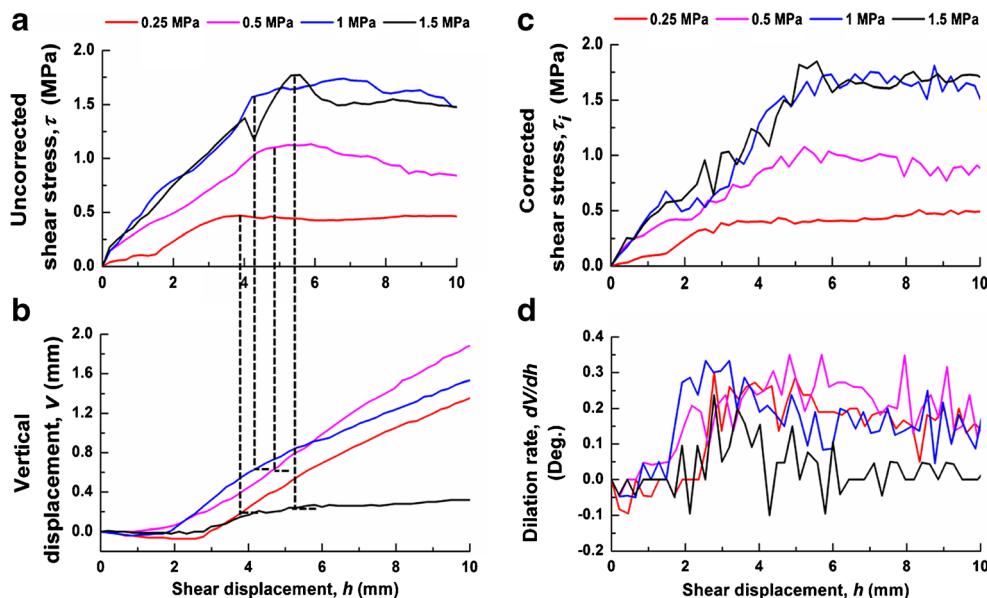
where  $i = \tan^{-1}(dv/dh)$  and  $dv$  and  $dh$  are vertical and horizontal displacements (0.2 mm), respectively. The Eq. (6) and Eq. (7) are for uphill movement of upper half of sample. The sign of these equations should be reverse in case of downhill movement.

In  $0^\circ$  direction of JR1, the dilation corrected shear stress ( $\tau_i$ ) and uncorrected shear stress ( $\tau_{exp}$ ) are compared for normal stress of 1.5 MPa (Fig. 3). It depicts that the trend of both plots is same, but in post-peak region, the  $\tau_{exp}$  is less than  $\tau_i$ . For this phenomenon, there may be two possible reasons. First is that the nominal area decreases sharply as the shearing progress and second is rate of dilation ( $dv/dh$ ) which may be positive due to failure of asperities and production of gouge material during shearing. For comparison, uncorrected peak shear stress ( $\tau_p$ ) and dilation-corrected peak shear stress ( $\tau_{ip}$ ) for 144 direct shear tests are reported in Table 4.

Table 5 Peak dilation angle ( $d_n$ ) and actual peak dilation angle ( $d_{na}$ )

Joint replica	Shearing direction	$\sigma_{n1} = 0.25$ MPa		$\sigma_{n2} = 0.5$ MPa		$\sigma_{n3} = 1$ MPa		$\sigma_{n4} = 1.5$ MPa	
		$d_n$ (Deg)	$d_{na}$ (Deg)	$d_n$ (Deg)	$d_{na}$ (Deg)	$d_n$ (Deg)	$d_{na}$ (Deg)	$d_n$ (Deg)	$d_{na}$ (Deg)
JR1	0	5.71	8.14	4.35	8.13	4.65	10.04	0.39	3.18
	30	1.89	3.77	5.38	12.09	2.46	4.97	3.90	6.50
	60	3.47	14.04	1.15	4.54	-1.15	5.44	-2.14	1.83
	90	3.43	16.26	-0.72	6.79	-0.19	10.30	-0.67	2.58
	120	3.43	5.89	-2.29	1.66	2.66	12.80	0.19	5.44
	150	1.68	5.71	3.01	4.33	1.91	6.34	-0.10	4.09
	180	7.97	12.75	2.98	8.65	0.71	2.60	-3.18	10.78
	210	5.14	12.68	6.42	25.46	2.58	26.57	1.43	13.42
	240	7.22	22.25	5.14	13.47	4.48	8.64	3.37	7.13
	270	-8.16	21.25	7.86	1.83	5.59	9.87	6.23	6.11
	300	6.65	18.84	5.51	17.82	4.95	10.65	0.57	4.09
	330	3.70	15.64	2.49	16.93	3.52	11.56	0.76	7.13
JR2	0	14.00	16.70	15.00	19.29	11.00	18.43	0.76	13.39
	30	18.26	19.86	14.75	17.65	12.13	15.26	11.45	13.84
	60	18.95	22.99	10.76	20.85	7.60	15.26	7.13	13.39
	90	8.90	19.05	8.53	12.80	4.29	10.78	2.38	7.77
	120	6.28	13.39	5.94	10.62	2.09	7.13	4.38	7.97
	150	6.03	21.80	7.75	12.09	6.29	10.78	6.10	10.78
	180	11.13	17.68	11.74	15.95	6.32	11.07	6.48	12.18
	210	16.44	18.43	9.93	14.68	8.31	11.31	4.29	8.13
	240	11.02	17.20	12.37	19.25	8.81	10.31	7.55	9.93
	270	10.29	14.85	10.58	22.04	9.13	10.78	7.69	13.39
	300	11.31	14.93	8.09	9.87	6.28	10.30	3.81	7.60
	330	12.95	15.38	12.32	14.68	10.48	13.39	9.65	14.49
JR3	0	8.62	14.35	7.97	13.39	0.86	7.58	0.57	5.13
	30	7.41	14.47	10.94	11.86	4.29	17.57	4.43	14.04
	60	12.27	13.39	10.11	15.96	8.34	11.75	7.97	12.06
	90	16.04	19.65	12.41	10.92	8.62	15.95	7.13	14.41
	120	14.57	15.95	13.76	18.82	12.81	13.39	8.63	10.26
	150	7.81	16.70	7.78	13.13	6.12	14.93	3.81	11.97
	180	9.20	14.62	5.71	7.41	6.09	7.91	4.86	12.09
	210	5.96	11.56	6.20	11.66	3.47	6.05	3.23	13.39
	240	8.40	12.80	8.84	12.80	7.69	11.07	5.60	9.46
	270	13.01	18.44	10.20	14.68	6.14	12.09	2.67	8.75
	300	11.13	15.22	10.76	15.26	3.78	9.46	1.43	4.97
	330	8.64	11.31	6.84	11.66	5.44	13.39	4.23	13.45

Fig. 4 Typical curves of direct shear test on JR2 in 0° direction



**Estimation of correct peak dilation angle**

Peak dilation angle is mobilized at peak shear stress and there is no peak dilation prior to peak shear stress and it is determined by drawing tangent at a point corresponding to peak shear stress ( $\tau_p$ ) on plot of vertical displacement versus shear displacement (Barton 1973). Hencher et al. (2011) exhibit that Barton’s approach is based on empiricism and provides instantaneous peak dilation angle. They suggested that peak dilation angle can exist prior or post to peak shear stress depending upon the nature of roughness and applied normal stress.

Therefore, to extend our understanding and to remove existing ambiguity toward peak dilation angle, Barton and Hencher’s approach are analyzed. In this paper, plots between uncorrected shear stress ( $\tau$ ) versus shear displacement ( $h$ ) (Fig. 4a), and vertical displacement ( $V$ ) versus shear displacement ( $h$ ) (Fig. 4b) are plotted. Then, peak dilation angle ( $d_n$ ) are determined as per Barton (1973). Moreover, the graphs between dilation-corrected shear stress ( $\tau_i$ ) versus shear displacement ( $h$ ) (Fig. 4c) and dilation rate ( $dv/dh$ ) versus shear

displacement ( $h$ ) (Fig. 4d) are drawn and actual peak dilation angle ( $d_{na}$ ) is determined. The values of  $d_n$  and  $d_{na}$ , are reported in Table 5 and observed that  $d_{na}$  underestimate the  $d_n$  at large extent. The reason for this phenomenon is that rate of dilation ( $dv/dh$ ) gives incremental dilation angle at every 0.2 mm shear displacement which is always high.

During analysis of data, multiple peaks of  $\tau_i$  is observed in Fig. 4c. However, in this research paper, first  $\tau_{ip}$  is recorded for all 144 direct shear tests. It is also noticed that concept of dilation rate ( $dv/dh$ ) provides easier way to find unique value of  $d_{na}$  in any shearing direction which is quite essential for prediction of peak shear stress of rock joints.

**Back calculated JRC**

Over the years, the prediction of *JRC* remains a matter of research to predict shear strength of rock joint in Barton’s model. So, it is imperative to know *JRC* in each shearing direction. For four normal stresses (0.25, 0.5, 1, 1.5 MPa),  $\tau_{Barton}$  is determined (Eq. 1) with one arbitrary value of *JRC*. Then, sum of square error (*SSE*) as given in Eq. (8) is minimized by altering the value of *JRC* in Solver add-in for Microsoft Excel. The value of *JRC* corresponding to minimum *SSE* is back calculated *JRC* in desire shear direction.

$$SSE = \sum (\tau_{exp} - \tau_B)^2 \tag{8}$$

As seen above, the back calculated *JRC* is determined after conducting direct shear tests at different normal stresses. But the ultimate aim is to find *JRC* in advance so that Barton’s model (Eq. 1) can be used in efficient way. Keeping this objective, efforts are made to predict back calculated *JRC* with known parameter of roughness ( $A_0$ ,  $\theta_{max}$ , and  $C$ ) in desired shearing direction. Different combinations of these parameters

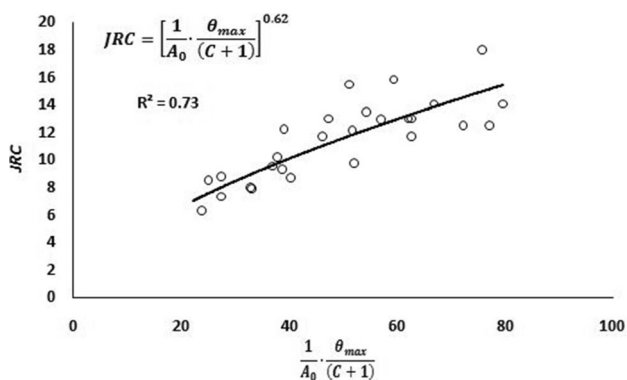
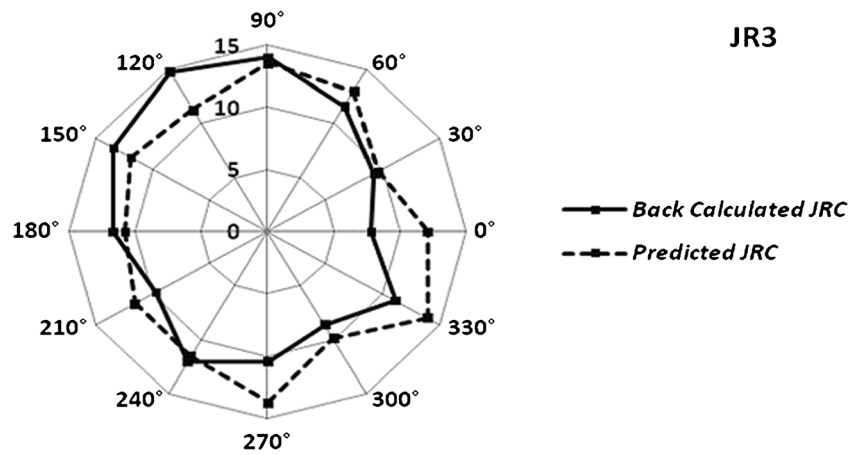


Fig. 5 Plot between *JRC* and  $\frac{1}{A_0} \times \frac{\theta_{max}}{(C+1)}$

**Fig. 6** Comparison between back calculated *JRC* and Predicted *JRC* for JR3



are plotted with back calculated *JRC* but they did not provide good relationships. Finally, back calculated *JRC* is plotted with function  $\frac{1}{A_0} \times \frac{\theta_{max}}{(C+1)}$  as shown in Fig. 5

and found that *JRC* can be predicted with power function ( $R^2 = 0.73$ ) as given in Eq. (9). For JR3, the back calculated *JRC* and predicted *JRC* are compared in radar

**Table 6** Dilation corrected peak shear strength ( $\tau_{ip}$ ) and predicted peak shear strength ( $\tau_{pre}$ ) of joint replicas

Joint replica	Shearing direction	$\sigma_{n1} = 0.25$ MPa		$\sigma_{n2} = 0.5$ MPa		$\sigma_{n3} = 1$ MPa		$\sigma_{n4} = 1.5$ MPa	
		$\tau_{ip}$	$\tau_{pre}$	$\tau_{ip}$	$\tau_{pre}$	$\tau_{ip}$	$\tau_{pre}$	$\tau_{ip}$	$\tau_{pre}$
JR1	0	0.46	0.33	0.56	0.61	1.37	1.13	1.55	1.61
	30	0.35	0.36	0.74	0.65	1.09	1.19	1.57	1.69
	60	0.39	0.36	0.52	0.66	1.15	1.20	1.09	1.70
	90	0.43	0.36	0.65	0.65	1.22	1.19	1.51	1.69
	120	0.38	0.33	0.53	0.61	1.09	1.13	1.58	1.61
	150	0.40	0.32	0.68	0.59	1.05	1.09	1.38	1.56
	180	0.56	0.31	0.67	0.57	1.28	1.07	1.92	1.53
	210	0.45	0.37	0.90	0.67	1.49	1.21	2.23	1.72
	240	0.52	0.38	0.91	0.69	1.25	1.24	1.69	1.76
	270	0.43	0.39	0.48	0.70	1.74	1.26	2.02	1.77
	300	0.56	0.32	0.79	0.59	1.33	1.10	1.64	1.58
	330	0.43	0.38	0.83	0.68	1.28	1.23	1.63	1.74
JR2	0	0.41	0.52	1.08	0.89	1.81	1.52	1.85	2.09
	30	0.61	0.69	1.07	1.09	1.67	1.78	2.56	2.40
	60	0.66	0.97	1.20	1.39	1.99	2.12	3.28	2.78
	90	0.49	0.41	0.88	0.73	0.97	1.30	1.97	1.82
	120	0.44	0.39	0.80	0.70	1.01	1.26	1.85	1.77
	150	0.54	0.52	0.73	0.89	1.44	1.52	2.25	2.10
	180	0.48	0.52	0.80	0.89	1.44	1.52	2.24	2.10
	210	0.45	0.50	0.64	0.85	1.64	1.48	2.06	2.04
	240	0.45	0.52	1.04	0.89	1.13	1.52	2.37	2.10
	270	0.43	0.58	0.92	0.97	1.48	1.63	2.45	2.22
	300	0.61	0.50	0.69	0.86	1.35	1.48	2.20	2.05
	330	0.65	0.72	0.93	1.13	1.80	1.83	2.66	2.45
JR3	0	0.43	0.33	0.74	0.61	1.08	1.13	1.55	1.61
	30	0.44	0.38	0.74	0.68	1.04	1.23	1.83	1.74
	60	0.59	0.46	0.89	0.80	1.01	1.41	1.90	1.96
	90	0.40	0.58	0.97	0.96	1.73	1.62	2.22	2.22
	120	0.65	0.64	1.33	1.03	1.67	1.71	2.22	2.32
	150	0.46	0.55	0.79	0.92	1.49	1.57	2.35	2.15
	180	0.48	0.46	0.73	0.81	1.12	1.41	2.24	1.96
	210	0.43	0.39	0.76	0.70	1.16	1.26	1.81	1.78
	240	0.35	0.48	0.84	0.83	1.53	1.44	1.99	2.00
	270	0.56	0.42	0.76	0.74	1.16	1.31	1.68	1.84
	300	0.44	0.36	0.91	0.65	1.26	1.18	1.45	1.68
	330	0.35	0.44	0.74	0.77	1.32	1.36	2.00	1.90
MSE(%)		1.33		2.11		3.75		4.95	



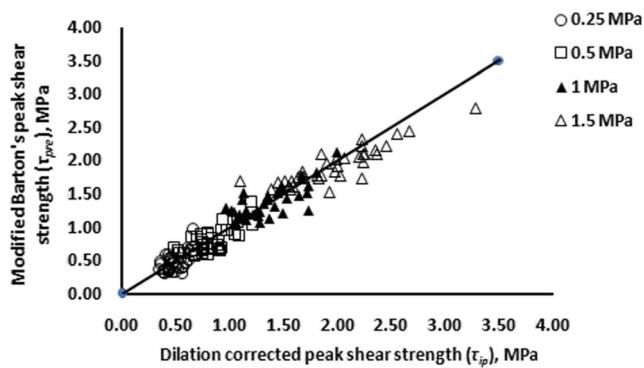


Fig. 7 Comparison between dilation corrected peak shear strength ( $\tau_{ip}$ ) and predicted shear strength ( $\tau_{pre}$ )

diagram (Fig. 6) which indicate that Eq. (9) provides the good approximation of *JRC*.

$$JRC = \left[ \frac{1}{A_0} \times \frac{\theta_{max}}{(C + 1)} \right]^{0.62} \quad (9)$$

### Modified Barton’s peak shear strength criterion ( $\tau_{pre}$ )

In order to develop peak shear strength criterion, it is assumed that shear behavior of rock joints replicas is similar to that of rock joints. Taking account this consideration, modified Barton’s peak shear strength criterion (Eq. 10) is developed by substituting Eq. (9) is in Eq.(1).

$$\tau_{pre} = \sigma_n \tan \left[ \phi_b + \left[ \frac{1}{A_0} \times \frac{\theta_{max}}{(C + 1)} \right]^{0.62} \times \log_{10} \left( \frac{JCS}{\sigma_n} \right) \right] \quad (10)$$

For all three joint replicas, dilation-corrected peak shear strength ( $\tau_{ip}$ ) and modified Barton’s peak shear strength

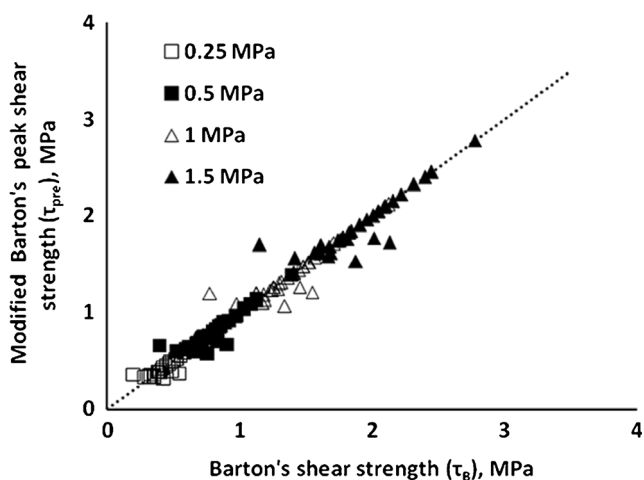


Fig. 8 Comparison of modified Barton’s peak shear strength criterion with Barton’s criterion

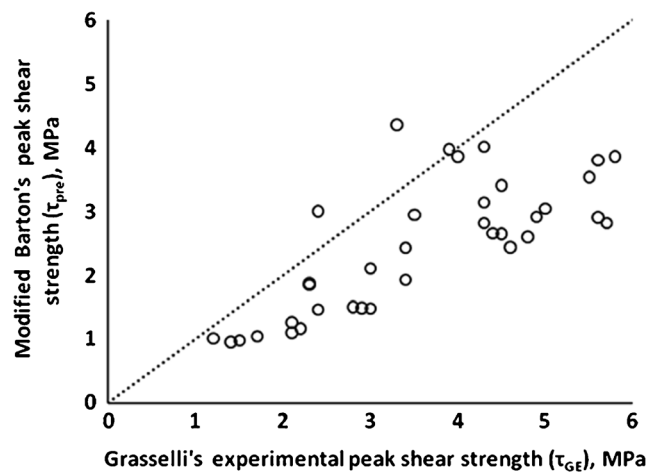


Fig. 9 Comparison of modified Barton’s peak shear strength with Grasselli’s experimental peak shear strength

( $\tau_{pre}$ ) are compared (Fig. 7). At each normal stress, mean square error (*MSE*) is calculated (Eq. 11) and the values of  $\tau_{ip}$  and  $\tau_{pre}$  with mean square error are listed in Table 6. It is noticed that mean square error varies from 1.33 to 4.95% which is quite reasonable.

$$MSE = \left[ \frac{1}{N} \sum_{i=1}^N (\tau_{ip} - \tau_{pre})^2 \right] \times 100 \quad (11)$$

### Comparison of modified Barton’s criterion with existing models

Modified Barton’s peak shear strength criterion is compared with Barton’s criterion as shown in Fig. 8. The mean square error (*MSE*) is calculated at normal stress of 0.25, 0.5, 1, and 1.5 MPa and found to be 0.24, 0.54, 1.22, and 1.93%, respectively, which is quite comparable.

Further, modified Barton’s peak shear strength criterion ( $\tau_{pre}$ ) is also compared with Grasselli’s experimental peak shear strength ( $\tau_{GE}$ ). For comparison, the input data like  $\sigma_n$ ,  $\phi_b$ ,  $A_0$ ,  $\theta_{max}$ ,  $C$ , and  $JCS$  are taken from the research paper of Grasselli and Egger (2003). It is found that for few experimental cases,  $\tau_{GE}$  overestimates the  $\tau_{pre}$  as shown in Fig. 9. The possible reason for overestimation may be that Grasselli and Egger (2003) calculated the joint roughness parameters  $A_0$ ,  $\theta_{max}$ , and  $C$  at accuracy of 0.05 mm, whereas in proposed modified Barton’s peak shear strength criterion, these parameters are calculated at accuracy of 0.10 mm. The another probable reason for this overestimation can be scale effect of joints because Grasselli and Egger (2003) have used joint size of 150 mm by 150 mm in lab experiments, whereas modified Barton’s peak shear strength criterion is proposed for joint sample of 90 mm diameter. However, the scale effect of joints is not studied in this manuscript.

## Conclusions

In this paper, 144 direct shear tests are performed on rock joint replicas of 90-mm diameter under constant normal load condition (CNL). In each shearing direction, experimental shear stress ( $\tau_{exp}$ ) is corrected using corrections like gross contact area ( $A_C$ ) and incremental dilation angle ( $i$ ). The peak dilation angle ( $d_n$ ) and actual peak dilation angle ( $d_{na}$ ) are determined with Barton's and incremental dilation ( $dv/dh$ ) approach, respectively. It is concluded that mostly numerical value of  $d_n$  is lower than the  $d_{na}$ . Therefore, this research recommends that the actual peak dilation should be determined by incremental dilation ( $dv/dh$ ) method.

A predictive model for  $JRC$  is developed based on morphological parameters like  $A_0$ ,  $\theta_{max}$ , and  $C$ . Finally, Barton's model is modified and it is observed that modified peak shear strength criterion provides good approximation of dilation corrected peak shear strength ( $\tau_{ip}$ ). The developed shear strength criterion has the advantage over existing models because it is independent of  $JRC$ . Modified Barton's peak shear strength ( $\tau_{pre}$ ) is compared with Barton's shear strength ( $\tau_B$ ) and found that  $\tau_{pre}$  closely matches with  $\tau_B$ . Moreover,  $\tau_{pre}$  is also compared with Grasselli's experimental shear strength ( $\tau_{GE}$ ) and it is found that few cases  $\tau_{GE}$  overestimate the values of  $\tau_{pre}$ . It is pointed out that the probable reasons of overestimation are scale effect and accuracy of joint roughness quantification in proposed model.

It should be noted here that parameters  $A_0$ ,  $\theta_{max}$ , and  $C$  are sensitive to measurement accuracy. Therefore, Eq. (9) is subjected to change at different measuring accuracy. The modified Barton's peak shear strength criterion is formulated for joint replicas by conducting laboratory direct shear tests in range of  $\sigma_n/\sigma_c=0.006$  to 0.036.

**Acknowledgments** The laboratory facilities, support, and suggestions of technical staff of Rock Mechanics Laboratory, IIT Kharagpur, India, for conducting necessary experiments is duly acknowledged.

## References

- Amadei B, Wibowo J, Sture S, Price RH (1998) Applicability of existing models to predict the behavior of replicas of natural fractures of welded tuff under different boundary conditions. *Geotech Geol Eng* 16:79–128. <https://doi.org/10.1023/A:1008886106337>
- Asadollahi P, Tonon F (2010) Constitutive model for rock fractures: revisiting Barton's empirical model. *Eng Geol* 113:11–32. <https://doi.org/10.1016/j.enggeo.2010.01.007>
- Barton N (1973) Review of a new shear-strength criterion for rock joints. *Eng Geol* 7:287–332. [https://doi.org/10.1016/0013-7952\(73\)90013-6](https://doi.org/10.1016/0013-7952(73)90013-6)
- Barton N, Choubey V (1977) The shear strength of rock joints in theory and practice. *Rock Mech* 10:1–54. <https://doi.org/10.1007/BF01261801>
- Barton N, Bandis S, Bakhtar K (1985) Strength, deformation and conductivity coupling of rock joints. *Int J Rock Mech Min Sci Geomech Abstr* 22:121–140. [https://doi.org/10.1016/0148-9062\(85\)93227-9](https://doi.org/10.1016/0148-9062(85)93227-9)
- Brown SR, Scholz CH (1985) Broad bandwidth study of the topography of natural rock surfaces. *J Geophys Res* 90:12575. <https://doi.org/10.1029/JB090iB14p12575>
- Ghazvinian AH, Azinfar MJ, Geranmayeh Vaneghi R (2012) Importance of tensile strength on the shear behavior of discontinuities. *Rock Mech Rock Eng* 45:349–359. <https://doi.org/10.1007/s00603-011-0207-9>
- Grasselli G, Egger P (2003) Constitutive law for the shear strength of rock joints based on three-dimensional surface parameters. *Int J Rock Mech Min Sci* 40:25–40. [https://doi.org/10.1016/S1365-1609\(02\)00101-6](https://doi.org/10.1016/S1365-1609(02)00101-6)
- Grasselli G, Wirth J, Egger P (2002) Quantitative three-dimensional description of a rough surface and parameter evolution with shearing. *Int J Rock Mech Min Sci* 39:789–800. [https://doi.org/10.1016/S1365-1609\(02\)00070-9](https://doi.org/10.1016/S1365-1609(02)00070-9)
- Hencher SR, Richards LR (1989) Laboratory direct shear testing of rock discontinuities. *Ground Eng* 22(2):24–31
- Hencher SR, Lee SG, Carter TG, Richards LR (2011) Sheeting joints: characterisation, shear strength and engineering. *Rock Mech Rock Eng* 44:1–22. <https://doi.org/10.1007/s00603-010-0100-y>
- Homand F, Belem T, Souley M (2001) Friction and degradation of rock joint surfaces under shear loads. *Int J Numer Anal Methods Geomech* 25:973–999. <https://doi.org/10.1002/nag.163>
- Huang SL, Oelke SM, Speck RC (1992) Applicability of fractal characterization and modelling to rock joint profiles. *Int J Rock Mech Min Sci Geomech Abstr* 29:89–98. [https://doi.org/10.1016/0148-9062\(92\)92120-2](https://doi.org/10.1016/0148-9062(92)92120-2)
- Huang et al (1993) An Investigation of the Mechanics of Rock Joints Part I. Laboratory investigation. *Int J Rock Mech Min Sci Geomech Abstr* 30:257–269
- ISRM (1978) International Society for Rock Mechanics commission on standardization of laboratory and field tests: suggested methods for the quantitative description of discontinuities in rock masses. *Int J Rock Mech Min Sci Geomech Abstr* 15(6):319–368
- Indraratna, Haque (2000) Shear behaviour of rock joint. Balkema, Rotterdam
- Jing L, Nordlund E, Stephansson O (1992) An experimental study on the anisotropy and stress-dependency of the strength and deformability of rock joints. *Int J Rock Mech Min Sci Geomech Abstr* 29:535–542. [https://doi.org/10.1016/0148-9062\(92\)91611-8](https://doi.org/10.1016/0148-9062(92)91611-8)
- Khosravi A, Sadaghiani MH, Khosravi M, Meehan CL (2013) The effect of asperity inclination and orientation on the shear behavior of rock joints. *Geotech Test J* 36:404–417
- Kulatilake PHSW, Um J (1999) Requirements for accurate quantification of self-affine roughness using the roughness-length method. *Int J Rock Mech Min Sci* 36:5–18. [https://doi.org/10.1016/S1365-1609\(98\)00170-1](https://doi.org/10.1016/S1365-1609(98)00170-1)
- Kulatilake PHSW, Shou G, Huang TH, Morgan RM (1995) New peak shear strength criteria for anisotropic rock joints. *Int J Rock Mech Min Sci Geomech Abstr* 32:673–697. [https://doi.org/10.1016/0148-9062\(95\)00022-9](https://doi.org/10.1016/0148-9062(95)00022-9)
- Kumar R, Verma AK (2016) Anisotropic shear behavior of rock joint replicas. *Int J Rock Mech Min Sci* 90:62–73. <https://doi.org/10.1016/j.ijmms.2016.10.005>
- Ladanyi B, Archambault G (1970) Simulation of shear behavior of jointed rock mass. In: 11th U.S. symposium on rock mechanics: theory and practice, Berkeley, California. pp. 105–125
- Li Y, Huang R (2015) Relationship between joint roughness coefficient and fractal dimension of rock fracture surfaces. *Int J Rock Mech Min Sci* 75:15–22. <https://doi.org/10.1016/j.ijmms.2015.01.007>
- Maerz NH, Franklin JA, Bennett CP (1990) Joint roughness measurement using shadow profilometry. *Int J Rock Mech Min Sci Geomech Abstr* 27:329–343. [https://doi.org/10.1016/0148-9062\(90\)92708-M](https://doi.org/10.1016/0148-9062(90)92708-M)
- Maksimović M (1992) New description of the shear strength for rock joints. *Rock Mech Rock Eng* 25:275–284. <https://doi.org/10.1007/BF01041808>

- Maksimović M (1996) The shear strength components of a rough rock joint. *Int J Rock Mech Min Sci Geomech Abstr* 33:769–783. [https://doi.org/10.1016/0148-9062\(95\)00005-4](https://doi.org/10.1016/0148-9062(95)00005-4)
- Milinverno A (1990) A simple method to estimate the fractal dimension of self-affine series. *Geophys Res Lett* 17:1953–1956
- Muralha J, Grasselli G, Tatone B, Blümel M, Chryssanthakis P, Yujing J (2014) ISRM suggested method for laboratory determination of the shear strength of rock joints: revised version. *Rock Mech Rock Eng* 47:291–302. <https://doi.org/10.1007/s00603-013-0519-z>
- Odling NE (1994) Natural fracture profiles, fractal dimension and joint roughness coefficients. *Rock Mech Rock Eng* 27:135–153. <https://doi.org/10.1007/BF01020307>
- Patton FD (1966) Multiple modes of shear failure in rock. In: *Proceedings of the 1st congress of the international society of rock mechanics*. Lisbon, Portugal, pp. 509–513
- Plesha ME, Ballarini R, Parulekar A (1989) Constitutive model and finite element procedure for dilatant contact problems. *J Eng Mech* 115(12):2649–2668
- Power WL, Tullis TE (1991) Euclidean and fractal models for the description of rock surface roughness. *J Geophys Res* 96:415. <https://doi.org/10.1029/90JB02107>
- Reeves MJ (1985) Rock surface roughness and frictional strength. *Int J Rock Mech Min Sci Geomech Abstr* 22:429–442. [https://doi.org/10.1016/0148-9062\(85\)90007-5](https://doi.org/10.1016/0148-9062(85)90007-5)
- Sakellariou M, Nakos B, Mitsakaki C (1991) On the fractal character of rock surfaces. *Int J Rock Mech Min Sci Geomech Abstr* 28:527–533
- Tatone BSA (2009) Quantitative characterization of natural rock discontinuity roughness in-situ and in the laboratory. University of Toronto, Toronto
- Tatone BSA, Grasselli G (2010) A new 2D discontinuity roughness parameter and its correlation with JRC. *Int J Rock Mech Min Sci* 47:1391–1400. <https://doi.org/10.1016/j.ijrmms.2010.06.006>
- Tse R, Cruden DM (1979) Estimating joint roughness coefficients. *Int J Rock Mech Min Sci Geomech Abstr* 16:303–307. [https://doi.org/10.1016/0148-9062\(79\)90241-9](https://doi.org/10.1016/0148-9062(79)90241-9)
- Wang JG, Ichikawa Y, Leung CF (2003) A constitutive model for rock interfaces and joints. *Int J Rock Mech Min Sci* 40:41–53. [https://doi.org/10.1016/S1365-1609\(02\)00113-2](https://doi.org/10.1016/S1365-1609(02)00113-2)
- Wibowo J, Amadel B, Sture S, Price RH (1994) Effect of boundary conditions on the strength and deformability of replicas of natural fractures in welded tuff: data analysis (No. SAND-93-7079). Sandia National Labs., Albuquerque, NM (United States); Colorado Univ., Boulder, CO (United States). Dept. of Civil, Environmental, and Architectural Engineering
- Xia CC, Tang ZC, Xiao WM, Song YL (2014) New peak shear strength criterion of rock joints based on quantified surface description. *Rock Mech Rock Eng* 47:387–400. <https://doi.org/10.1007/s00603-013-0395-6>
- Xie H, Wang JA, Kwaśniewski MA (1999) Multifractal characterization of rock fracture surfaces. *Int J Rock Mech Min Sci* 36:19–27. [https://doi.org/10.1016/S1365-1609\(98\)00172-5](https://doi.org/10.1016/S1365-1609(98)00172-5)
- Yang Z, Chiang D (2000) An experimental study on the progressive shear behavior of rock joints with tooth-shaped asperities. *Int J Rock Mech Min Sci* 37:1247–1259. [https://doi.org/10.1016/S1365-1609\(00\)00055-1](https://doi.org/10.1016/S1365-1609(00)00055-1)
- Yang ZY, Di CC (2001) A directional method for directly calculating the fractal parameters of joint surface roughness. *Int J Rock Mech Min Sci* 38:1201–1210. [https://doi.org/10.1016/S1365-1609\(02\)00006-0](https://doi.org/10.1016/S1365-1609(02)00006-0)
- Yang ZY, Lo SC, Di CC (2001) Reassessing the joint roughness coefficient (JRC) estimation using Z2. *Rock Mech Rock Eng* 34:243–251. <https://doi.org/10.1007/s006030170012>
- Yu X, Vayssade B (1991) Joint profiles and their roughness parameters. *Int J Rock Mech Min Sci Geomech Abstr* 28:333–336. [https://doi.org/10.1016/0148-9062\(91\)90598-G](https://doi.org/10.1016/0148-9062(91)90598-G)
- Zhao J (1997a) Joint surface matching and shear strength. Part a: joint matching coefficient (JMC). *Int J Rock Mech Min Sci Geomech Abstr* 34:173–178. [https://doi.org/10.1016/S0148-9062\(96\)00062-9](https://doi.org/10.1016/S0148-9062(96)00062-9)
- Zhao J (1997b) Joint surface matching and shear strength. Part B: JRC-JMC shear strength criterion. *Int J Rock Mech Min Sci Geomech Abstr* 34:179–185. [https://doi.org/10.1016/S0148-9062\(96\)00063-0](https://doi.org/10.1016/S0148-9062(96)00063-0)